07 Dec 2005

Experimental Study of the Solids Velocity Field in Gas-Solid Risers

Satish Bhusarapu

Muthanna H. Al-Dahhan
Missouri University of Science and Technology, aldahhanm@mst.edu

Milorad P. Duduković

Steven Trujillo

et. al. For a complete list of authors, see https://scholarsmine.mst.edu/che_bioeng_facwork/1311

Recommended Citation

Experimental Study of the Solids Velocity Field in Gas−Solid Risers

**Satish Bhusarapu,[†,§] Muthanna H. Al-Dahhan,[†] Milorad P. Duduković,*,[†]
Steven Trujillo,[‡] and Timothy J. O'Hern[‡]**

*Chemical Reaction Engineering Laboratory, Department of Chemical Engineering, Washington University,
Campus Box 1198, 1 Brookings Drive, St. Louis, Missouri 63130-4899, and Engineering Sciences Center,
Sandia National Laboratories, MS 0834, P.O. Box 5800, Albuquerque, New Mexico 87185*

Solids flow dynamics in gas−solid risers is inherently complex. Model refinement through experimental validation requires the acquisition of detailed nonintrusive measurements. In this study, noninvasive computer-automated radioactive particle tracking (CARPT) is employed to visualize and quantify in a three-dimensional domain the solids dynamics and mixing in gas−solid risers. This technique has the added advantage that, along with the derived Eulerian solids flow field (time-average velocity map and various turbulence parameters such as the Reynolds stresses, turbulent kinetic energy), it also provides directly the Lagrangian description of the solids motion. The solids velocity field data are obtained in two different risers at low and high solids fluxes at varying superficial gas velocity to span both the fast-fluidized (FF) and dilute phase transport (DPT) regimes. The effect of operating conditions on solids flow and mixing is studied. Comparative analysis of the results is presented to provide insights into the complex solids flow patterns characteristic of gas−solid risers.

1. Introduction

Circulating fluidized beds (CFB) exhibit very complex dynamics caused by interactions between the gas and solids phases. As revealed in earlier studies (e.g., Bader et al.;[1] Pita and Sundaresan;[2] Davidson;[3] Parssinen and Zhu[4]), the motion of solids is driven by many mechanisms that are difficult to identify and to quantify. From an engineering viewpoint, the operating conditions determine the solids flow and mixing, which in turn influence the performance of CFBs. Academic researchers in the last decades acquired considerable knowledge about local solids hydrodynamics in CFB units close to walls at low solids fluxes when these systems can be observed by optical techniques. On the other hand, industrial practice emphasized high flux systems such as fluid catalytic cracking (FCC) units and CFB combustors. The modeling effort, starting with the model of Sinclair and Jackson,[5] revealed a remarkably rich variety of behavior of gas−solid flow in a vertical pipe over the range of possible flow conditions. There is still considerable uncertainty and disagreement with regard to the dependence of fine scale structures on the operating conditions. This dependency is important in scale-up, design, and optimization. In this study, an attempt is made to ascertain the effect of operating conditions on the solids flow field parameters such as solids velocity, turbulent stresses, and granular temperature and on mixing parameters such as residence times, circulation times, and local and global dispersion coefficients.

Generally in CFBs, to maximize profitability, gas and solids residence times are chosen to achieve the highest product yield per unit volume. In FCC units, a short and uniform catalyst residence time in the riser reactor, with reduced backmixing, leads to better reactor performance (larger amounts of desired products and/or a higher conversion) by reducing the inventory of the deactivated catalyst in the riser. In other words, a uniform radial profile of solids velocity and little solids backmixing in the riser is preferred, leading to shorter and more uniform solids residence times. Solids residence time distribution (RTD) in the riser is also important in noncatalytic gas−solid reactions, as in a combustor, since this characterizes the degree of solids mixing and provides information about the physical properties of solid particles in the riser. In addition, lateral mixing and internal recirculation of solids in a CFB combustor are necessary to maintain uniform temperatures over the entire length of the riser. Hence, lateral and longitudinal mixing is advantageous in a CFB combustor, while in a FCC unit axial mixing is disadvantageous. The following question arises: How do the operating conditions affect the solids axial and radial holdup and the solids residence time? In addition, high gas velocities and low solids holdup are preferred in some applications to minimize compressor costs. However, for many catalytic reactions, lower gas velocities may be preferred because they give higher solids holdup, thus maximizing specific activity per unit volume (Berruti et al.[6]). This raises another question: How does one achieve the specific flow structure required for a specific application by varying the operating conditions, reactor design, or particle characteristics?

To answer such questions, it is necessary to have a fundamental understanding of the particle flow mechanism in risers. Existing models describing this complex flow often lack *relevant* experimental data needed for model validation and refinement (Berruti et al.;[6] Sinclair[7]). Moreover, many of the phenomenological and CFD models require empirical inputs, and their quality depends on the availability and accuracy of the measurement techniques and data. Hence, to answer the above questions, and to properly understand the solids

---

* To whom correspondence should be addressed. Tel.: (314) 935-6021. Fax: (314) 935-4832. E-mail: dudu@wustl.edu.
† Washington University.
‡ Sandia National Laboratories.
§ Present address: Harper International Corp., West Drullard Ave., Lancaster, NY 14086.

flow inside risers, it is first necessary to map the solids flow field inside a pilot-scale riser.

Several researchers employed invasive methods such as pitot tubes, extraction probes, isokinetic probes, spatial filter processes, and optical fiber probes to characterize mean radial velocity profiles (Bader et al.;[1] Miller and Gidaspow;[8] Harris et al.;[9] Fiedler et al.;[10] Parssinen and Zhu[4]). Some noninvasive methods used were based on optical techniques such as PIV, LDV, and high-speed cameras (Rhodes et al.;[11] Wang et al.[12]), while a few others were based on the use of radio-isotopes, such as PEPT (Stellema[13]) and radioactive particle tracking (Godfroy et al.[14]). Most of the above studies provide only the time-averaged solids velocity profiles at few axial locations, while only a very few provide three-dimensional (3-D) velocity components in 3-D columns. None of the previous studies provide turbulence stresses or turbulent kinetic energy (granular temperature), which are required to characterize the local and global solids mixing in the riser. We attempt to systematically gather and present all this information in the present work.

2. Experimental Section

Glass beads with density of $\rho_p = 2.5$ g cm^{-3} and a Sauter mean diameter of 150 μm (with a standard deviation of about 15 μm) were employed in the experiments. A ^{46}Sc radionuclide, tailored to match the density of the glass beads and the Sauter mean diameter of the solids, was employed as a tracer. To match the size and density of the beads, a Sc particle of size 136 μm was coated with a 7 μm thick polymer, parlyene N. While the size and density of the tracer particle matched perfectly the size and density of the beads in the riser, the restitution coefficient was not measured and was assumed comparable. The position of this single tracer in the riser was monitored at a sampling rate of 5 ms (i.e., frequency of 200 Hz). Further details regarding the computer-automated radioactive particle tracking (CARPT) technique and ability to provide time-averaged velocities (3-D solids flow field) and turbulence parameters (kinetic energy, shear stress, turbulent eddy diffusivities) can be found elsewhere (Lin et al.;[15] Moslemian;[16] Devanathan;[17] Larachi et al.;[18] Degaleesan[19]).

The studies were performed in two different CFB systems and risers. One is with riser dimensions of 6 in. i.d. (15.2 cm) and 26 ft (7.93 m) tall and with a downcomer of 2 in. i.d. (5.1 cm), installed at the Chemical Reaction Engineering Laboratory (CREL) to obtain data at low solids fluxes ($G_s < 40$ kg·m^{-2}·s^{-1}). Further details of the setup can be found in Bhusarapu.[20] The CARPT experiments were performed in a section considered to experience close to fully developed flow (in a time-averaged sense) at an axial height from 5 to 5.7 m. This corresponds to a dimensionless axial height (Z/D) of 32.8−37.4.

The second riser is part of the CFB setup at Sandia National Laboratory (SNL) as shown in Figure 1. CARPT experiments on this setup acquired solids velocity data at high solids flux conditions ($G_s > 100$ kg m^{-2} s^{-1}). Solids are fed from the 28 cm inside diameter (i.d.) downcomer through a metering valve and a standpipe into the riser engagement section. Air is vented at the top of this standpipe to the low-pressure region in the freeboard of the downcomer. The engagement section at the riser's base is an annular arrange-
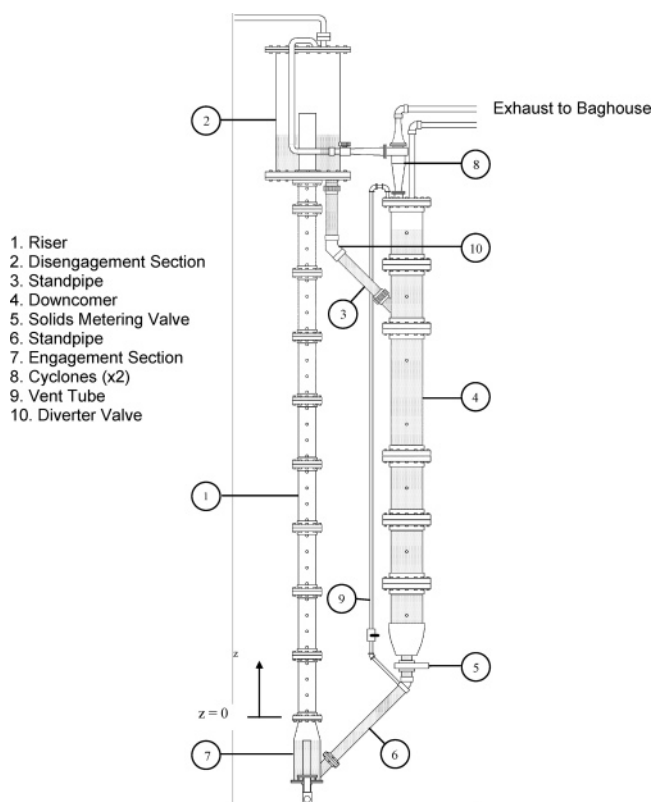

1. Riser
2. Disengagement Section
3. Standpipe
4. Downcomer
5. Solids Metering Valve
6. Standpipe
7. Engagement Section
8. Cyclones (x2)
9. Vent Tube
10. Diverter Valve

Exhaust to Baghouse

Figure 1. Schematic of the CFB setup at SNL.

Table 1. Operating Conditions and Regimes for Flow Measurements[a]

	CREL			SNL		
U_g^{riser} (m s^{-1})	3.2	3.9	4.5	5.49	5.56	7.71
G_s (kg m^{-2} s^{-1})	26.6	30.1	32.1	102	145	119
regime	FF	DPT	DPT	DPT/FF	FF	DPT
G_s (kg m^{-2} s^{-1})	30.1	33.7	36.8			
regime	FF	DPT	DPT			

[a] FF, fast fluidization; DPT, dilute phase transport.

ment, with the particles forming a fluidized bed surrounding a central 8.5 cm diameter air supply pipe. Motive air entrains particles from the fluidized bed and transports them up the 14 cm i.d. riser column to the particle disengagement section. In the disengagement section, a flat aluminum plate normal to the flow turns the flow, acting as an inertial particle separator. Particles thus separated fall into a fluidized bed at the base of the disengagement section. This bed empties back to the downcomer through an underflow standpipe. The motive air and any unseparated particles exit the top of the disengagement section through two parallel transport lines to cyclone separators installed on top of the downcomer. The motive air and any remaining particles exit the cyclones and are vented to the atmosphere through a HEPA filter baghouse. The riser has a total length of 5.77 m of uniform diameter, or an aspect ratio of about $L/D \sim 41$. The zone of investigation for the CARPT experiments was at axial heights between 2.08 and 2.79 m with a dimensionless height (Z/D) between 14.9 and 20. The annular design of both the engagement and disengagement sections is to ensure that the flow in the vertical riser is as axisymmetric as possible. The riser is extensively grounded to reduce triboelectric effects. Motive air is supplied to the riser from large compressors. The supply pressure is reduced from 1700 to 480 kPa by a two-stage regulator, and air
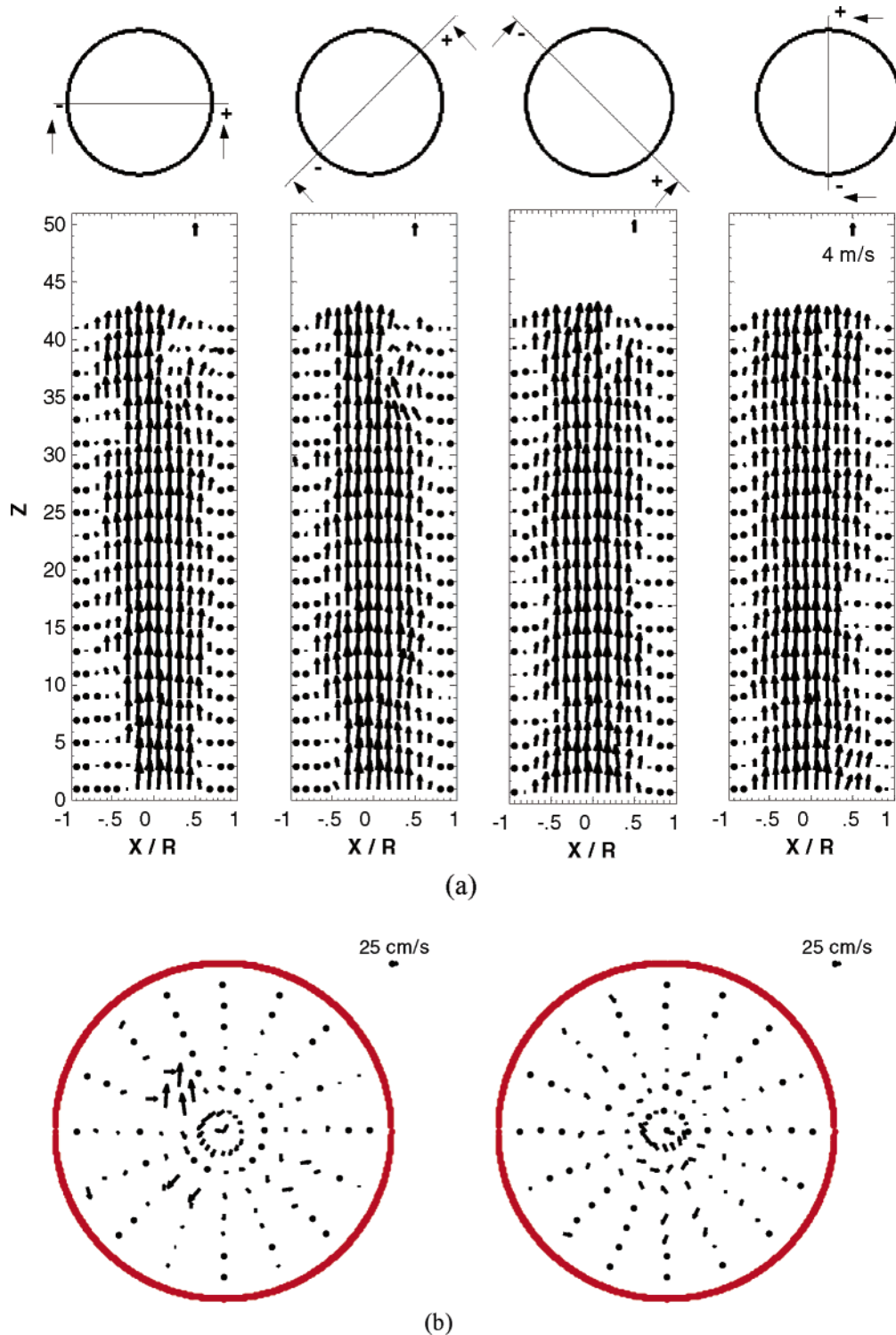
(a)

(b)

Figure 2. Visualization of solids velocity vectors in the zone of interrogation in (a) $r-z$ plane at different angles; (b) $r-\theta$ plane at different axial heights ($z/D = 16.3, 18.5$). FF regime at $U_g = 5.6$ m s^{-1}; $G_s = 144.5$ kg m^{-2} s^{-1}.

flow is controlled by a ball valve. Fluidization air is supplied to the CFB loop at the bases of the downcomer, the engagement section, and the disengagement section, and in the solids transfer standpipes. Depending on the location of application, fluidization air flow is controlled either manually or by a combination of thermal mass-flow meter/controller units. An orifice plate upstream of the riser inlet is used to monitor the motive-air flow rate. Motive-air temperature and humidity are also measured at this location. Typical temperatures are 17−

19 °C and typical relative humidity is 15%; uncertainties in these quantities are ±1 °C and ±1%, respectively.

Flow Regimes. The details of the operating conditions are shown in Table 1. The overall solids mass flux was determined using the method described in Bhusarapu et al.[21] Once the operating parameters such as superficial gas velocity (U_g^{riser}) and overall solids mass flux (G_s) have been estimated, one can determine the flow regime of operation. A circulating fluidized bed is generally operated between the gas choking velocity
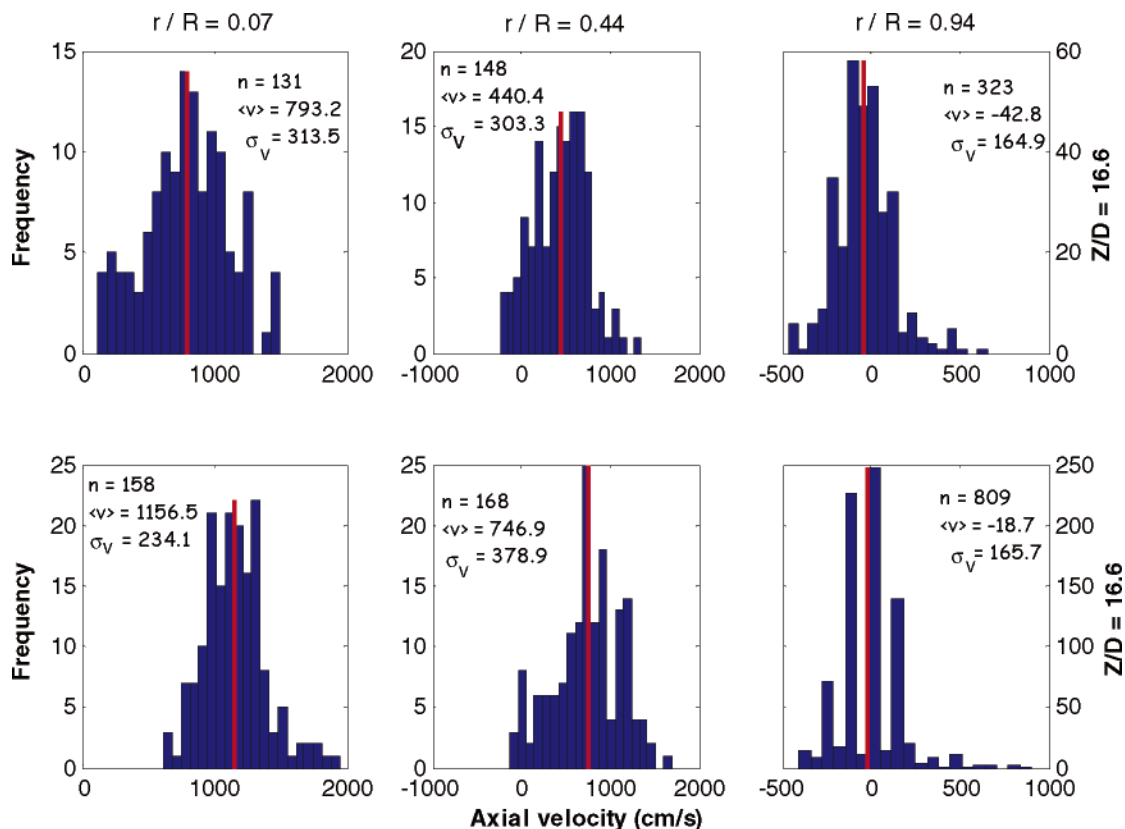
Figure 3. Probability density functions of axial solids velocity at three radial locations: (a, top) FF ($U_g = 5.5$ m s^{-1}; $G_s = 144$ kg m^{-2} s^{-1}); (b, bottom) DPT ($U_g = 7.7$ m s^{-1}; $G_s = 119$ kg m^{-2} s^{-1}). Each of the PDFs shown represents a simple voxel at the indicated radial and axial position with a fixed angular position.

(Bi and Grace[22]) and the gas velocity close to the minimum pressure gradient point. As given in Table 1, the operation in both the CREL (low flux) and SNL (high flux) risers cover the fast fluidization (FF) and the core−annular dilute phase transport (represented as DPT for convenience) regimes. Solids velocity fields and circulation patterns are determined by CARPT at the specified operating conditions (Table 1) in these two regimes.

3. Results and Discussion

Solids Velocity Fields. In a CARPT experiment, the position of the single radioactive tracer particle in 3-D space is determined at every "instant" (i.e., at every 0.005 s). Time differencing of these positions results in Lagrangian velocity traces. Ensemble averaging of several such Lagrangian velocity traces results in an ensemble-averaged Eulerian velocity field and allows estimation of turbulence parameters. Such interpretation inherently assumes that the system is ergodic (Moslemian;[16] Devanathan[17]). Ergodicity is defined as relating to a process in which every sizable sample is equally representative of the whole. Before discussing the solids velocity field results obtained from such an assumption, one needs to validate it post facto. This is performed by checking the velocity and turbulence quantities for occurrence independence. The flow parameters displayed occurrence independence (beyond 70% data) for all the operating conditions investigated. In addition, one needs to compartmentalize the zone of interrogation for converting the multiple Lagrangian traces of the single particle to ensemble-averaged Eulerian flow field of the ensemble of particles. To

obtain mesh-independent velocity and turbulence quantities, different mesh sizes were considered. A mesh given by the nominal grid size of $\Delta r = 0.95$ cm, $\Delta z = 2$ cm, and $\Delta\theta$ varied, so that all the cells had equal volume of about 5.7 cm^3, resulted in mesh-independent profiles. Further details on occurrence and mesh independence of the flow variables can be found in Bhusarapu.[20] In addition, the mean velocity fields, when visualized in $r-z$ and $r-\theta$ planes (Figure 3), revealed an axisymmetric flow structure of the solids for the flow conditions (Table 1) investigated.

Figure 2 reveals relatively small ensemble-averaged radial and azimuthal velocity components (compared to axial) as expected in fully developed flow. The axial variation of the ensemble-averaged velocity vectors is less than 13%, indicating a close to fully developed flow in a time-averaged sense. Completely fully developed solids flow cannot be inferred from Figure 2 in a strict sense, since the radial velocities are only relatively small and are numerically not equal to zero. The radial variation of the velocity vectors in Figure 3 indicates that solids are flowing upward in the central core and that solids are moving downward in an outer annulus. This represents the core (up) and annulus (down) flow structure often postulated in the literature. Such strong radial variation can indeed be seen from the ensemble averages of the solids axial velocity probability density functions (PDFs) shown in Figure 3. The axial velocity PDFs in both flow regimes display significant negative velocities also present near the wall transitioning to no negative velocities at the center of the column. This solids flow pattern at high solids fluxes is in contrast to that in the low solids flux flow conditions (not shown for brevity), where velocity PDFs reveal a bimodal axial
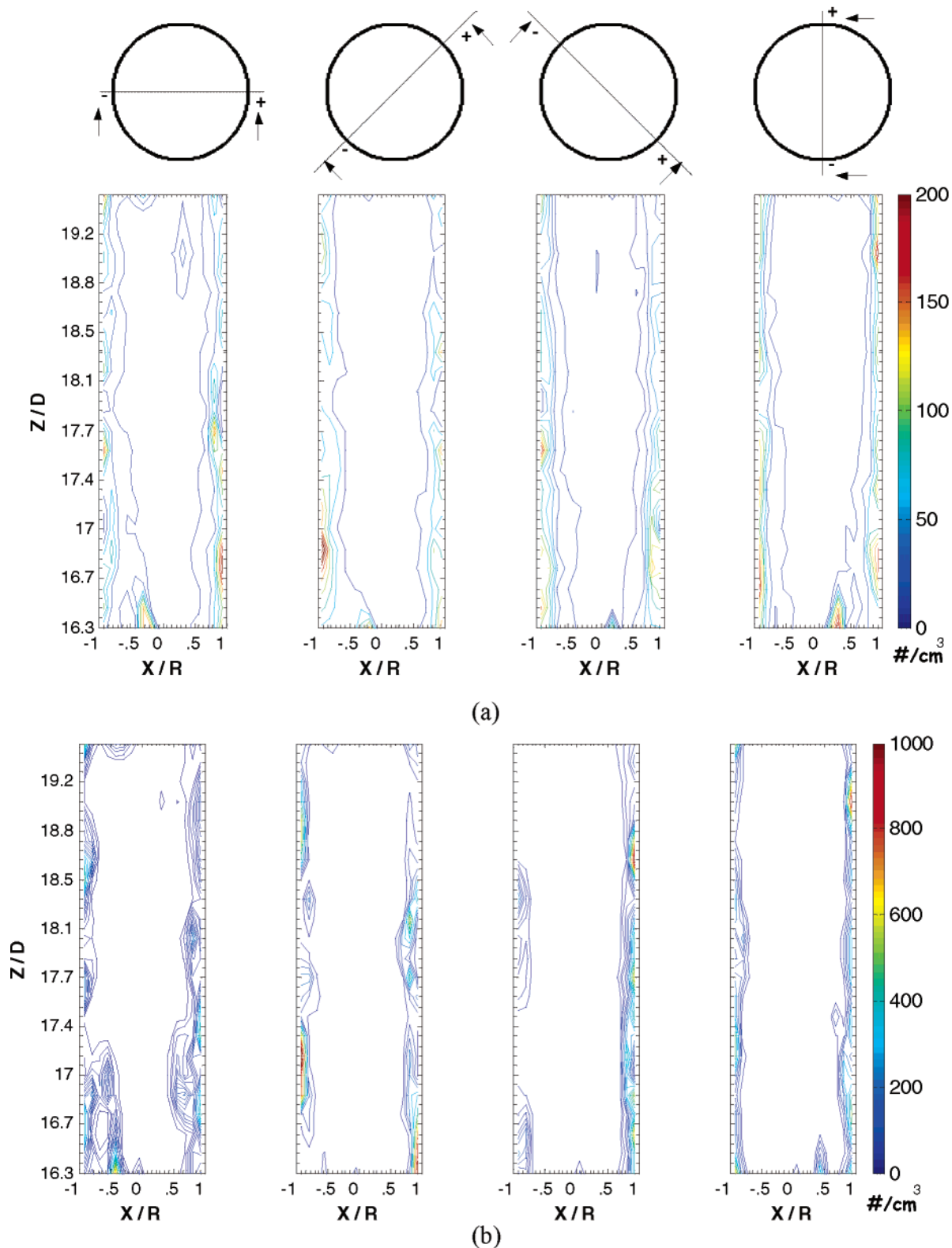
Figure 4. Contour plots (visualized at different longitudinal views) of particle occurrences per unit volume (#/cm^3): (a) FF regime (U_g^{riser} = 5.56 m s^{-1}; G_s = 144.5 kg m^{-2} s^{-1}) and (b) DPT (U_g^{riser} = 7.71 m s^{-1}; G_s = 119 kg m^{-2} s^{-1}).

velocity PDF with negative velocities near the center. The negative axial velocities at the center were interpreted to be due to clusters falling down (Bhusarapu et al.[23]). Hence, in contrast to the low flux conditions, a clustering phenomenon either does not seem to occur in the central core at high flux conditions under FF

regime or does not lead to downward traveling clusters in the core.

In the DPT regime (Figure 3b), at high solids flux the ensemble-averaged solids axial velocities near the wall are negative, which was not the case in the low flux conditions. This is probably due to the increase in the
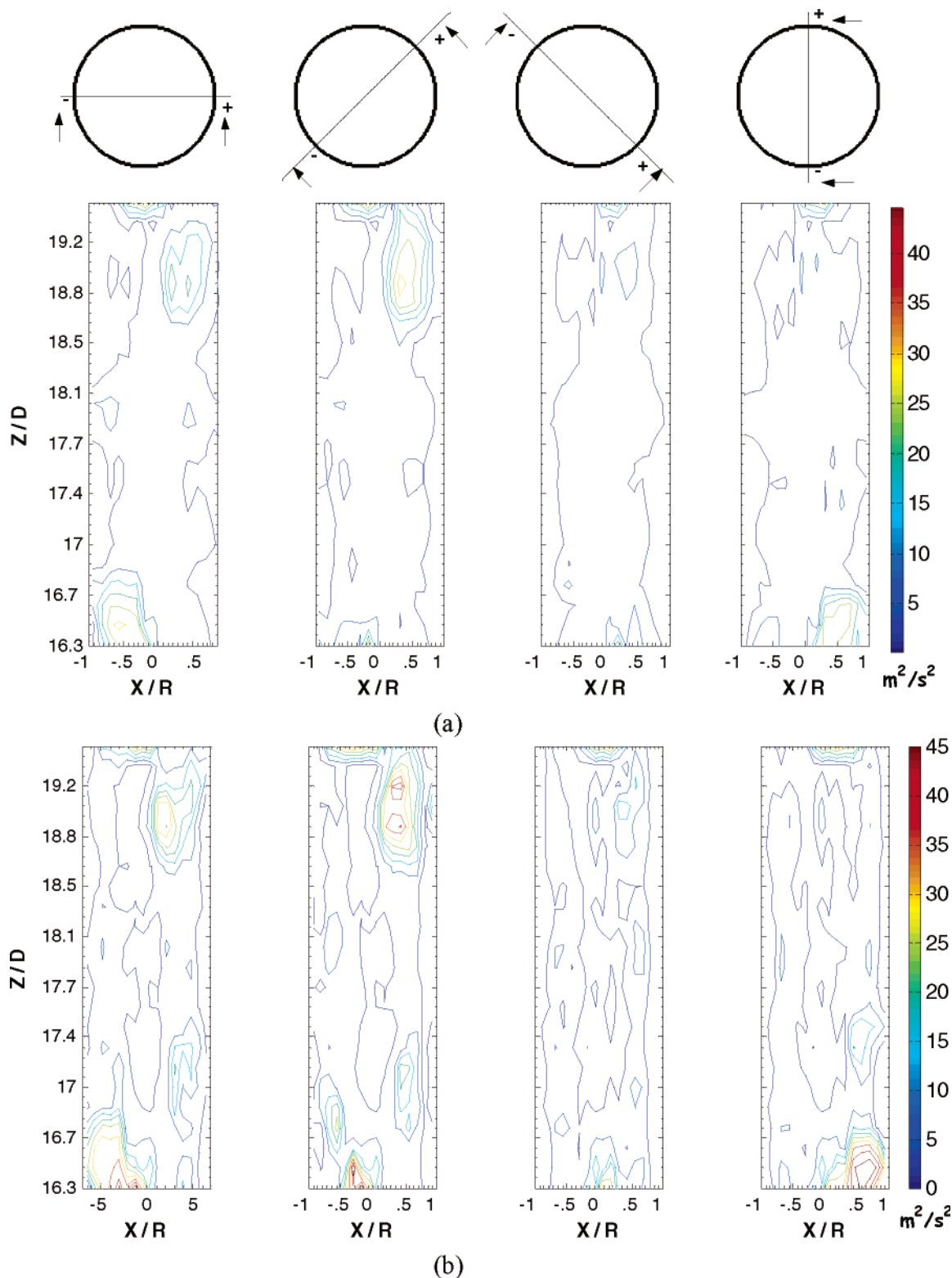
Figure 5. Contour plots (visualized at different longitudinal views) of turbulent kinetic energy per unit bulk density: (a) FF regime ($U_g^{riser} = 5.56$ m s^{-1}; $G_s = 144.5$ kg m^{-2} s^{-1}) and (b) DPT ($U_g^{riser} = 7.71$ m s^{-1}; $G_s = 119$ kg m^{-2} s^{-1}).

solids concentration at high solids flux, resulting in increased tendency for clustering near the wall which in turn increases the downflow. Thus, the velocity PDFs from FF and DPT regimes suggest that the clustering phenomenon is localized near the walls at high solids fluxes, while it is common throughout the riser cross section (FF regime) at low solids fluxes.

Particle occurrence profiles, when visualized in different $r-z$ planes as shown in Figure 4, indicate close

to axisymmetric flow of solids. Radial segregation seems to be intense in both FF and DPT regimes at high solids fluxes. Annulus thickness indicated by the contours in Figure 4 was found to be higher in the FF regime as compared to that in the DPT regime. The annulus thickness increases with the increasing solids flux at constant gas superficial velocity ($U_g^{riser} = 5.5$ m s^{-1}; $G_s = 102$, 144.5 kg m^{-2} s^{-1}). In contrast to no annulus found at low solids flux conditions, the DPT regime at
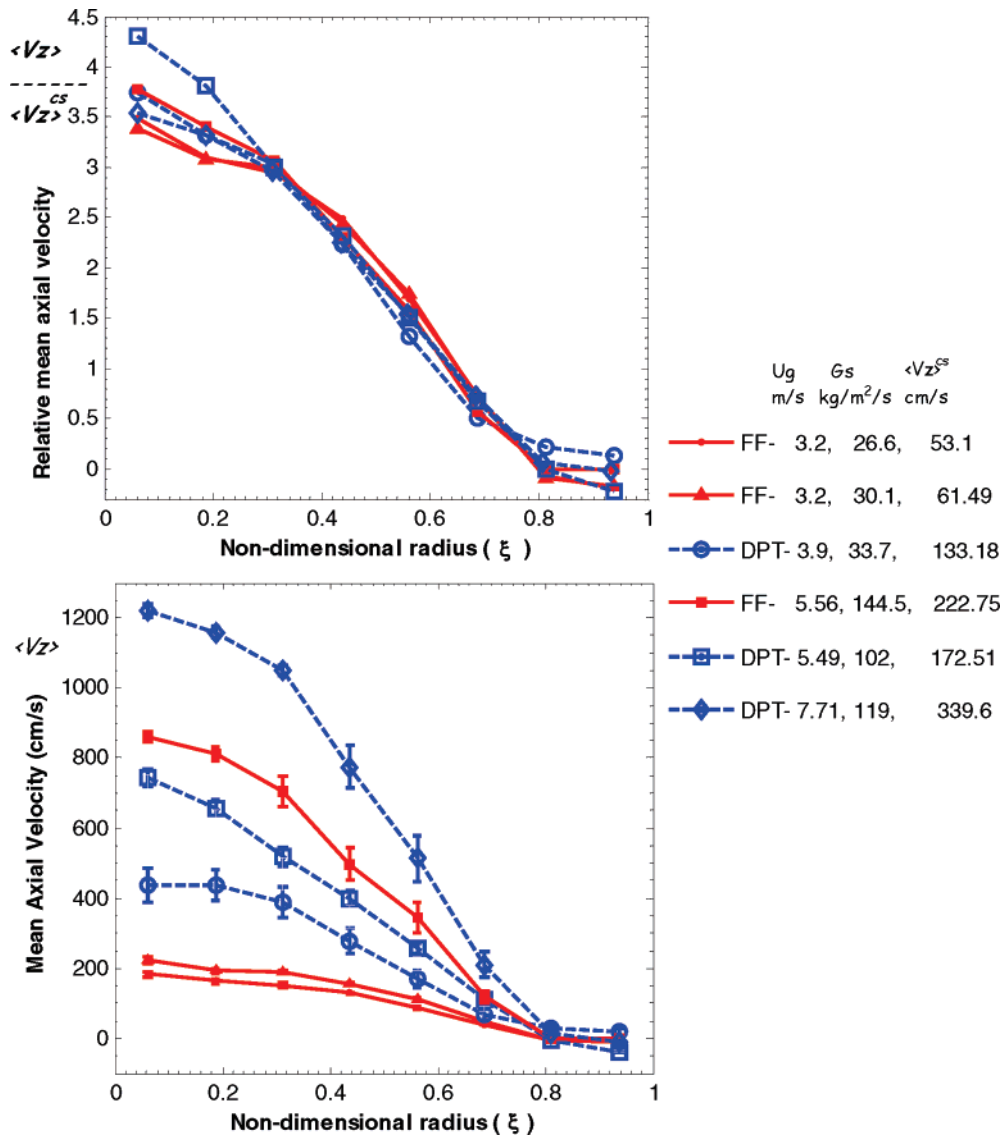
Figure 6. Circumferentially and axially averaged time-averaged radial profiles of (a, top) relative solids axial velocity and (b, bottom) solids axial velocity for all flow conditions investigated. The data were obtained from two different risers, at low solids fluxes in the CREL riser and at high solids fluxes in the SNL riser.

high solids flux conditions exhibits a dense film of solids close to the walls moving downward (Figure 4b). Although the total number of particle occurrences was different in each of the flow conditions in Figure 4a and 4b, the magnitudes of the values in the contours suggest that the annulus is denser and thinner in the DPT regime, while it is less concentrated and thicker in the FF regime. This result indicates that radial segregation is more severe in the DPT regime at high solids fluxes (beyond a certain solids volume fraction limit). At low solids fluxes negligible radial segregation was observed in the DPT regime. absence of any contour lines in the central core region, in both the FF and DPT regimes, indicates the presence of a relatively very small and uniform solids concentration in the core region. Thus, solids aggregation tendency or cluster formation is negligible in the core region at high solids fluxes, which supports the conclusion from the velocity PDFs.

Contour plots of turbulent solids kinetic energy per unit bulk density, shown in Figure 5, suggest an approximately axisymmetric turbulent field in both the FF and DPT regimes. Comparing Figures 4 and 5, profiles of turbulent kinetic energy seem to correlate

well with those of the particle occurrences in the FF regime (similarity to the gas holdup). However, in the DPT regime such similarity is not observed.

Mean Radial Profiles of Solids Velocity. Contour plots in the previous section displayed an axisymmteric flow structure inside risers. Also, the axial variation in the flow parameters was negligible, indicating the flow to be close to fully developed in the zone of investigation. Hence, all the profiles were azimuthally and axially averaged so as to investigate the effect of operating conditions on the one-dimensional flow structure in risers.

Figure 6 displays the radial profiles of the ensemble-averaged and spatially averaged solids velocity in the axial direction for all operating conditions investigated. To assess the similarity in the mean axial velocity profiles, the velocities were normalized in Figure 6a with the corresponding cross-sectional averaged values reported in the legend. Figure 6a suggests that the shapes of the mean axial velocity profiles are similar in both risers at low and high solids fluxes. This result is in agreement with the "similar profiles" concept of Monceaux et al.[24] and Rhodes et al.,[11] where both
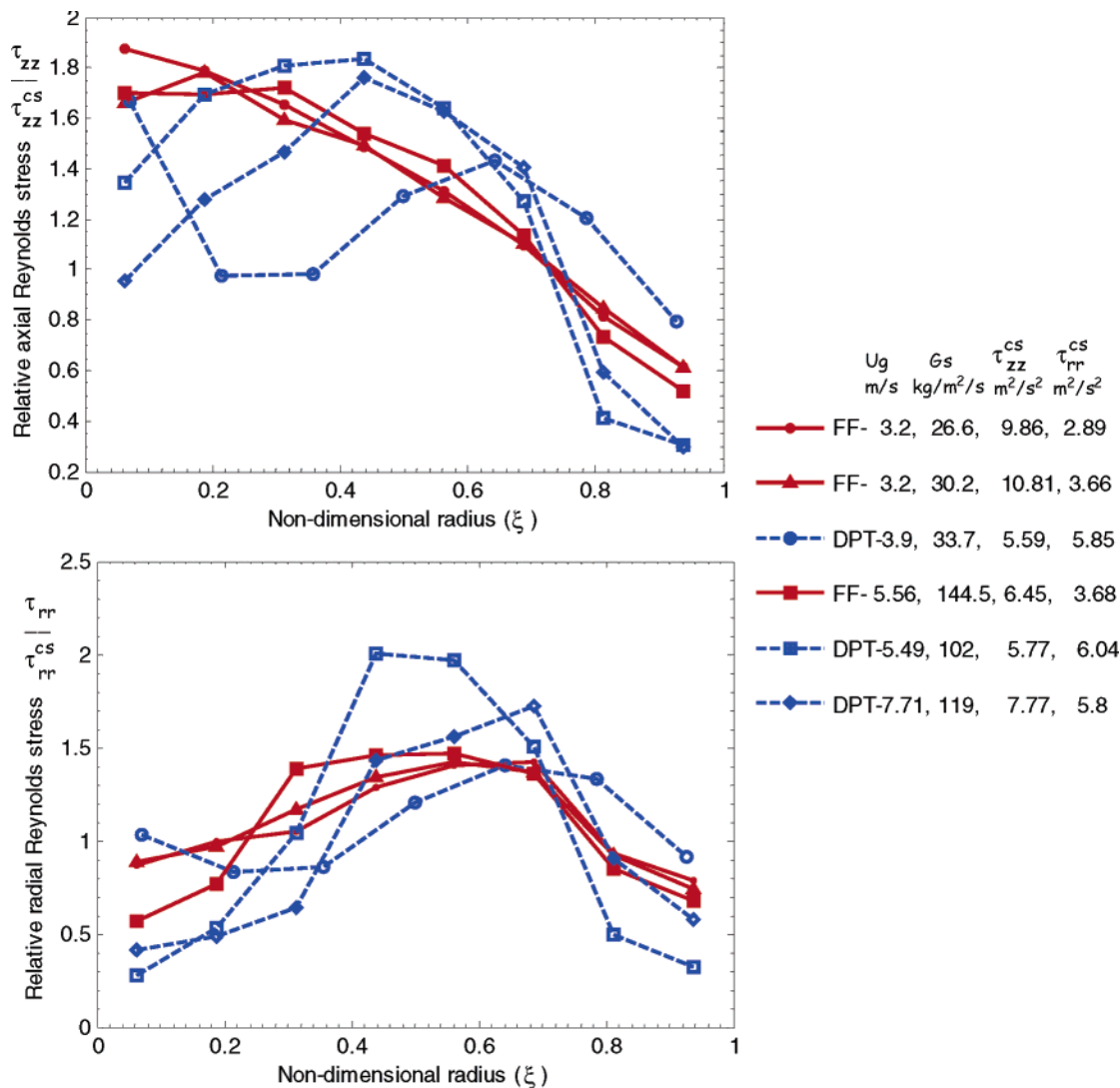
Figure 7. Circumferentially and axially averaged radial profiles of relative Reynolds normal stresses in (a, top) axial and (b, bottom) radial directions for all flow conditions investigated. Data at low solids fluxes from the CREL riser and at high solids fluxes from the SNL riser.

studies showed that, at a given gas velocity, radial profiles of the relative solids mass flux changed very little with the changes in the mean solids flux in the riser. The relative solids holdup profiles also varied very little under the same operating conditions, as reported by Bhusarapu et al.[20] Hence, both the time-averaged relative solids axial velocity and the solids holdup profiles for a range of operating conditions investigated can be described with a single functional form for each. Berruti et al.[6] speculated that such "similar profiles of mass flux" may be valid over a very limited range of operating conditions. Although solids mass flux cannot be determined accurately from time-averaged solids velocity and solids holdup profiles (due to the lack of the cross-correlation values), our results seem to be in near agreement with the concept of Monceaux et al.[24] and Rhodes et al.[11]

The flow condition at $U_g^{riser} = 5.5$ m s^{-1} and $G_s = 102$ kg m^{-2} s^{-1}, however, exhibits a slightly different functional form near the center (Figure 6a). This deviation is probably because of the flow being close to regime transition, resulting in the oscillating flow of the suspension, moving in slugs.

The mean solids axial velocity, as seen in Figure 6b, increases with the increase in mass flux at constant gas

velocity, which agrees with the most of the reported studies (for example, Berruti et al.[6]). A substantial increase in the mean solids axial velocity is observed in the center of the flow when superficial gas velocity and mass flux were increased from the FF to the DPT regime (Figure 6b). Within the spatial resolution of the velocity reconstruction, the inversion point of the solids axial velocity profile (corresponding to annulus thickness) was found to be in the same compartment (with $r/R = 0.81$). Hence, the downflow of solids at the wall is expected to cause considerable backmixing in the solids phase. It can also be observed from Figure 6b that the error bars indicated on the velocities are relatively small (within 15%), supporting the earlier conclusion of solids flow being close to fully developed.

Radial Profiles of Turbulent Parameters. The radial profiles of relative axial and radial normal solids stresses are shown in Figure 7. The axial normal solids Reynolds stress seems to decay in the radial direction monotonically in the FF regime, while in the DPT regime it peaks at an intermediate radial position and then decays radially. The above trend seems to persist at both the low and high solids fluxes. The cross-sectional average of the solids axial normal stress increases with the increase in the solids flux at constant
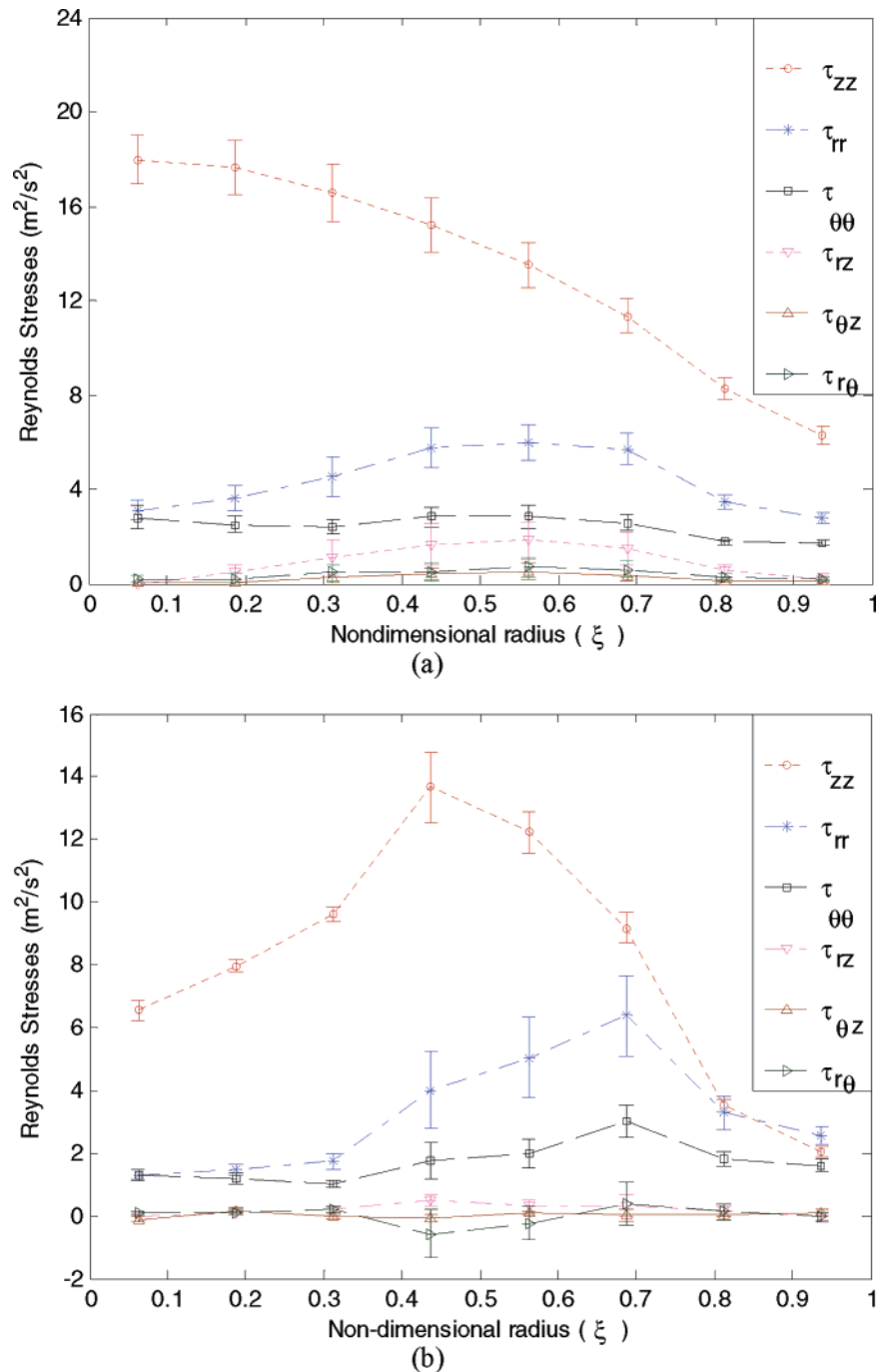
Figure 8. Circumferentially and axially averaged radial profiles of Reynolds stresses in (a) FF regime ($U_g^{riser} = 3.2$ m s^{-1}; $G_s = 26.6$ kg m^{-2} s^{-1}) and (b) DPT regime ($U_g^{riser} = 7.71$ m s^{-1}; $G_s = 119$ kg m^{-2} s^{-1}).

gas velocity. Note that the operating condition at $U_g^{riser} = 5.49$ m s^{-1} and $G_s = 102$ kg m^{-2} s^{-1} is indicated as DPT, while it is very close to the regime transition velocity (Figure 2). Interestingly, the radial normal stress for all the flow conditions shows a peak close to the radial position of $r/R = 0.7$. The reason could be that this radial position is the interface at which the flat and low solids holdup profile, prevalent in the core region, starts to increase drastically with radius toward the wall. Hence, the radial particle exchange between the dilute core and dense wall region is extensive at this interface. It can be noticed that the cross-sectional average of the solids radial normal stress increases with solids flux at low solids flux conditions, while it decreases with solids flux at high solids flux conditions.

The reasons for such a trend in solids Reynolds stresses are discussed below along with the trends for granular temperature.

Spatially averaged radial profiles of the six components of Reynolds stress tensor are plotted in Figure 8. Clearly, turbulence in both the FF and DPT regimes (parts a and b, respectively, of Figure 8) is anisotropic. The solids azimuthal normal stress is much smaller than the axial and radial normal components in both flow regimes, and their profiles seem to look relatively flat. The shear stress, τ_{rz}, is found to be 1 order of magnitude smaller than the normal stresses. The radial profiles of the solids shear stress, as noticed in Figure 8, show a peak near the radial position $r/R = 0.5$ and tend to zero near the center and the walls. A similar
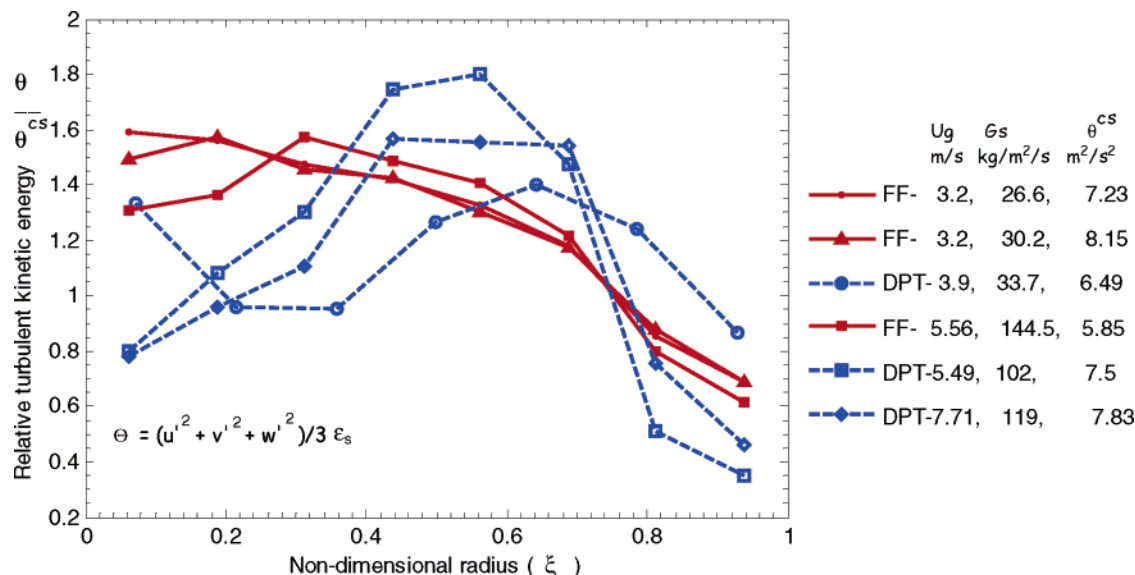
Figure 9. Circumferentially and axially averaged radial profiles of relative turbulent solids kinetic energy per unit bulk density for the flow conditions in FF and DPT regimes.

trend was observed for all the operating conditions from both risers (CREL and SNL). These results for solids shear stress are in agreement with the data and simulations reported by Tartan and Gidaspow.[25] The solids shear stress is found to increase with the increasing solids flux at both the low and high solids fluxes. The angular components of the shear stress, $\tau_{\theta r}$ and $\tau_{z\theta}$, can be observed from Figure 8 to be negligible and are considered zero.

The granular temperature in kinetic theory of granular flows, when scaled by a constant, represents the turbulent kinetic energy of solids. The radial profiles of the turbulent kinetic energy (per unit bulk density) for all the operating conditions are displayed in Figure 9. The contribution from the azimuthal component is much smaller than that from the axial and radial components, indicating the strong anisotropic nature of turbulence.

The contribution of the axial fluctuations dominates, and hence the granular temperature profiles are similar to the respective axial normal stress profiles. The granular temperature in the FF regime decreases in the radial direction monotonically, while it shows a peak in the DPT regime. Such a trend can be observed at both low and high solids flux conditions. The granular temperature increases with the increasing solids flux at constant gas velocity at low solids flux conditions, while it decreases with the increasing solids flux at high flux conditions. It was argued by Bhusarapu et al.[23] that the relative dominance of the increase in particle collision frequency over the decrease of the mean free path with increasing solids concentration dictates the trends in granular temperature. A decrease in the gas velocity or an increase in the solids flux increases the particle concentration. The results shown in Figure 9 support the hypothesis that particle fluctuations increase with concentration in "dilute conditions" ($\epsilon_s < 0.01-0.06$) and decrease beyond some solids holdup limit. Tartan and Gidaspow[25] reported that in dilute conditions the granular temperature peaks at an intermediate radial location. The trends in Figure 9 suggest that despite the solids concentration being higher, such a peak in the granular temperature occurs in the DPT regime.

4. Summary and Conclusions

The uniqueness of CARPT data lies in providing rich Lagrangian information along with the ensemble-averaged Eulerian flow field. The effect of operating conditions on the local solids velocity field required for the design and scale-up and for the CFD closures are addressed in this work. Following are the key conclusions with regard to the solids flow and mixing in gas–solid risers operated in the FF and DPT regimes:

(i) The clustering phenomenon (if present) is localized near the walls at high solids fluxes, while it is common throughout the riser cross section (FF regime) at low solids fluxes.

(ii) Radial solids segregation is more severe in the DPT regime at high solids fluxes (beyond a certain solids volume fraction limit). Solids aggregation tendency or cluster formation is negligible in the core region at high solids fluxes.

(iii) The shapes of the mean solids axial velocity profiles are similar for risers at low and high solids fluxes, agreeing with the "similar profiles" concept of Monceaux et al.[24] and Rhodes et al.[11]

(iv) The cross-sectional average of the mean axial solids velocity was found to increase with the increase in solids mass flux at constant gas velocity.

(v) The granular temperature in the FF regime decreases in the radial direction monotonically, while it shows a peak in the DPT regime.

(vi) Granular temperature was found to increase with solids concentration at "dilute conditions" ($\epsilon_s < 0.01-0.06$) and decrease beyond certain solids holdup.

In summary, the solids backmixing characterized by several mixing parameters aided in understanding the solids mixing mechanisms and the effect of operating conditions. Kinetic theory should benefit from these data as it needs to be extended to realistic anisotropic description of the riser solids flow phenomena.

Acknowledgment

Notation

d_p = particle diameter (m)
D = diameter of the column (m)
G_s = mass flux (kg m^{-2} s^{-1})
r = radial position (cm)
R = riser radius (cm)
t = time (s)
U_g^{riser} = superficial gas velocity (m s^{-1})
u' = fluctuating velocity (m s^{-1})
z = axial distance (m)

Greek Letters

ϵ_s = holdup
ρ = density (kg·m^{-3})
σ = standard deviation
τ = stress tensor per unit bulk density (m^2 s^{-2})
Θ_s = turbulence kinetic energy (m^2 s^{-2})
ξ = dimensionless radius

Subscripts and Superscripts

g = gas
s = solid phase
p = particle
z = axial
r = radial
θ = azimuthal
ρ = density
cs = cross-sectional average

Literature Cited

(1) Bader, R.; Findlay, J.; Knowlton, T. M. Gas/Solid flow patterns in a 30.5 cm diameter circulating fluidized bed riser. *Circulating Fluidized Bed Technology III*; Basu, P., Large, J. F., Eds.; Pergamon Press: New York, 1988; pp 123−137.

(2) Pita, J. A.; Sundaresan, S. Developing flow of gas-particle mixture in a vertical riser. *AIChE J.* **1993**, *39*, 541−555.

(3) Davidson, J. F. Circulating Fluidized Bed Hydrodynamics. *Powder Technol.* **2000**, *113* (3), 249−260.

(4) Parssinen, J. H.; Zhu, J. X. Particle velocity and flow development in a long and high-flux circulating fluidized bed riser. *Chem. Eng. Sci.* **2001**, *56*, 5295−5303.

(5) Sinclair, J. L.; Jackson, R. Gas particle flow in a vertical pipe with particle-particle interaction. *AIChE J.* **1989**, *35*, 1473−1486.

(6) Berruti, F.; Chaouki, J.; Godfroy, L.; Pugsley, T. S.; Patience, G. S. Hydrodynamics of Circulating Bed Risers: A Review. *Can. J. Chem. Eng.* **1995**, *73*, 579−601.

(7) Sinclair, J. L. CFD for Multiphase Flow: Research codes and commercial software. *AIChE Symp. Ser.* **2000**, *323*, 138−146.

(8) Miller, A.; Gidaspow, D. Dense, Vertical Gas-Solid Flow in a Pipe. *AIChE J.* **1992**, *38* (11), 1801−1815.

(9) Harris, B. J.; Davidson, J. F.; Xue, Y. Axial and radial variation of flow in Circulating Fluidized Bed Risers. *Circulating Fluidized Bed Technology IV*; Avidan, A. A., Ed.; American Institute of Chemical Engineers: New York, 1993; pp 103−110.

(10) Fiedler, O.; Werther, J.; Labahn, N.; Kumpart, J.; Christofori, K. Measurement of local particle velocities and velocity distributions in gas-solid flows by means of spatial filter method. *Powder Technol.* **1997**, *94*, 51−57.

(11) Rhodes, M. J.; Wang, X. S.; Cheng, H.; Hirama, T.; Gibbs, B. M. Similar profiles of solids flux in circulating fluidized bed risers. *Chem. Eng. Sci.* **1992**, *47*, 1635−1643.

(12) Wang, T.; Lin, Z. J.; Zhu, C. M.; Liu, D. C.; Saxena, S. C. Particle velocity measurements in a circulating fluidized bed. *AIChE J.* **1993**, *39*, 1406−1410.

(13) Stellema, C. S. Radiotracers for Gas/Solids Flows in (Interconnected) Fluidized Beds. Ph.D. Dissertation, Delft University of Technology, Delft, The Netherlands, 1998.

(14) Godfroy, L.; Larachi, F.; Chaouki, J. Position and velocity of a large particle in a gas/solid riser using the radioactive particle tracking technique. *Can. J. Chem. Eng.* **1999**, *77*, 253−261.

(15) Lin, J. S.; Chen, M. M.; Chao, B. T. A Novel Radioactive Particle Tracking Facility for Measurement of Solids Motion in Gas Fluidized Beds. *AIChE J.* **1985**, *31*, 465−473.

(16) Moslemian, D. Study of solids motion, mixing and heat transfer in gas-fluidized beds. Ph.D. Thesis, University of Illinois at Urbana−Champaign, Urbana, IL, 1987.

(17) Devanathan, N. Investigation of Liquid Hydrodynamics in Bubble Columns via a Computer Automated Radioactive Particle Tracking (CARPT) Facility, D.Sc. Thesis, Washington University, Saint Louis, MO, 1991.

(18) Larachi, F.; Kennedy, G.; Chaouki, J. A γ-ray Detection System for 3-D Particle Tracking in Multiphase Reactors. *Nucl. Instrum. Methods Phys. Res., Sect. A* **1994**, *338* (2−3), 568−576.

(19) Degaleesan, S. Fluid Dynamic Measurements and Modeling of Liquid Mixing in Bubble Columns, D.Sc. Thesis, Washington University, Saint Louis, MO, 1997.

(20) Bhusarapu, S. Solids Flow Mapping in a Gas-Solid Riser, D.Sc. Thesis, Washington University, Saint Louis, MO, 2005.

(21) Bhusarapu, S.; Fongarland, P.; Al-Dahhan, M. H.; Duduković, M. P. Measurement of Overall Solids Mass Flux in a Gas-Solid Circulating Fluidized Bed. *Powder Technol.* **2004**, *148* (2−3), 155−168.

(22) Bi, H. T.; Grace, J. R. Flow regime diagrams for gas-solid fluidization and upward transport. *Int. J. Multiphase Flows* **1995**, *21*, 1229−1236.

(23) Bhusarapu, S.; Al-Dahhan, M. H.; Duduković, M. P. Solids Flow Mapping in a Gas-Solid Riser: Mean Holdup and Velocity Fields. *Powder Technol.* **2006**, in press.

(24) Monceaux, L.; Azzi, M.; Molodtsof, Y.; Large, J. F. Overall and local characterization of flow regimes in a circulating fluidized bed. *Circulating Fluidized Bed Technology*; Basu, P., Ed.; Pergamon Press: New York, 1986; pp 185−191.

(25) Tartan, M.; Gidaspow, D. Measurement of granular temperature and stresses in risers. *AIChE J.* **2004**, *50* (8), 1760−1775.